Applied Physics A: Materials Science & Processing manuscript No.
(will be inserted by the editor)

Mechanical, structural and scaling properties of coals: Depth-sensing indentation studies

Elena L. Kossovich[1], Feodor M. Borodich[2], Svetlana A. Epshtein[1], Boris A. Galanov[3], Maxim G. Minin[4], Vera A. Prosina[1] ⋆

[1] National University of Science and Technology 'MISiS' 4, Leninsky prospekt, Moscow, 119049, Russian Federation

[2] School of Engineering, Cardiff University, Cardiff, CF24 3AA, UK

[3] Frantsevich Institute of Materials Science Problems, National Academy of Sciences of Ukraine, vul. Krzhizhanovskogo 3, Kiev, 03680 Ukraine

[4] Ural Federal University named after the first President of Russia B.N.Yeltsin, 19, Mira street, Ekaterinburg 620002, Russian Federation

Received: date / Revised version: date

Abstract This paper discusses special features of mechanical behaviour of coals discovered using depth-sensing indentation (DSI) techniques along with other traditional methods of material testing. Many of the special features are caused by the presence of multiscale complex heterogeneous internal structure within the samples and brittleness of some coal components. Experimental methodology for studying mechanical properties of coals and other natural extreme materials like bones are discussed. It is argued that values of microhardness of bituminous coals correlate strongly with the maximum load, therefore the use of this parameter in application to coals may be meaningless. For analysis of the force-displacement curves obtained by DSI, both Oliver-Pharr and Galanov-Dub approaches are employed. It is argued that during nanoindentation, the integrity of the internal structure of a coal sample within a small area of high stress field near the tip of indenter may be destroyed. Hence, the standard approaches to mechanical testing of coals should be re-examined.

Key words Natural extreme materials, Coals, Hardness, Nano-indentation, Size effect

⋆ Research was supported by the Russian Science Foundation (grant #16-17-10217)

1 Introduction

We report the results of studies of mechanical properties of coals. The term 'coal' cannot be attributed to a specific material having well known material properties, but this is a wide class of materials having extremely complex heterogeneous internal structure formed by geological processes. Distinctive varieties of coals include brown coals (also known as "lignites"), bituminous coals (also known as "steam coal", "rock coals" and "hard coals") and anthracite. The heterogeneity of coals exists at many length scales from the nanoscale to the macroscale. The internal structure defines specific features of the physical and mechanical properties of coals. Like rocks consisting of various minerals, coals are composed of many distinct organic entities called macerals and some amount of inorganic substances along with internal pores and cracks. The organic part of coals contains from 65 to 95% carbon depending on the degree of the coal metamorphism. The maceral composition of coals is defined by many factors such as history of the coalification processes, the nature of the initial plant material and the conditions of its accumulation and decomposition [1–3]. Due to sedimentary nature of coals, their lamination is identified at different scales: from seams (coal strata) [2] to micron and submicron sizes [3]. Hence, it is reasonable to model coals as 3D micro- or even nano-scale composites having rather hierarchical heterogeneous structures.

Due to presence of inhomogeneous internal structure and clear scaling properties of coals, they can be considered as a class of natural extreme materials. The term 'extreme materials' has been introduced recently to characterise materials having internal micro-structures and/or hierarchically organized architectures at different scales, that demonstrate drastically enhanced physical characteristics at macroscale (extreme macroscopic characteristics) due to the underlying arrangements of their structural elements. Using techniques of depth-sensing indentation (DSI) at nano and micro levels, we demonstrate that mechanical characteristics of coals determined employing the classic approaches demonstrates scaling properties. For example, the hardness of a coal maceral determined using microindentation differs considerably of hardness values of the same maceral determined using nanoindentation. Here, we show that contrary to other natural extreme materials like some biomaterials, e.g. bone elements, where traditional treatment of DSI tests are applicable, the traditional approaches to hardness of materials and interpretation of DSI data may be meaningless in application to coals.

Mechanical properties of coals were usually measured by standard large-scale tests. These tests include compression both uniaxial [4–6] or triaxial [5,7,8], tension [9, 10], bending [11], cutting [12] and microhardness (Vickers) indentation [13–15]. Acoustic emission tests are also actively employed to characterize coals elastic properties and performance under external mechanical effects

[16–19]. Even these traditional methods revealed some anomalous behavior of coals. For example, traditionally coals are modelled as elastic brittle materials. However, it was shown that they may also demonstrate the distinguished stages of deformation process and transitions of their characteristics analogous to plastic materials [16]. Further, stiffness and flexural strength of the strip-shaped samples extracted from the one chunk of coal may vary in an extremely large range; this fact was explained by existence of defects in the samples that are not visible by optical microscopy [11]. In addition, mechanical properties of coals demonstrate anisotropy with respect to the bedding direction [5, 17, 18]. There exist an assumption that coals could be treated as laminated structures [20] with unknown toughness of interfaces between separate layers (thickness of which may vary from several meters to nanometers [3, 21]). Some approaches on investigation of interface toughness could be of use when considering of thin (micro- to nanometers) coals layers [22,23]. Coals formation conditions (including underground pressure of overburden strata) are the reason for existence of internal stresses in their matter [21]. It is also known that the DSI curves may be significantly affected by residual stresses (see, e.g. [24, 25]). Acoustic emission of coals shows also anomalously high level [16]. Even at microscale, it is difficult to obtain the repeatable results due to high heterogeneity of samples and differences between mechanical properties of different macerals [13].

Let us discuss the indentation testing of coals. In many countries including Russia, the microhardness tests are performed according to the official standards [15] that, in turn, assume the use the standard PMT-3 device. For microhardness testing of metals, Khrushchov and Berkovich [26] introduced two devices: the PMT-2 and the PMT-3 that are in essence special versions of the Vickers indenters. Although Khrushchov and Berkovich introduced the use of three-side pyramidal indenters [27], and Berkovich suggested further to use a three-sided indenter that has the same relation between the cross-section area A at height h as the Vickers indenter has, i.e. $A \approx 24.5h^2$; the PMT-3 device is based on the use of a diamond Vickers pyramid that produces a square imprint and the microhardness is calculated by the size of the imprint's diagonal measured by optical microscopy. The microhardness value is calculated as

$$H = \frac{2P \sin \frac{\alpha}{2}}{d^2},$$

where d is the average diagonal of the imprint, P is the load acting on the pyramid indenter, and α is the apex angle between the opposite faces of pyramid. For a Vickers pyramid $\alpha = 136^\circ$. The procedures of microhardness tests are well known; they are regulated either by the Russian standard [15] used in application to coals by many countries of the former Soviet Union or by ASTM standard [28] that was created mainly for the applications to metals.

In 2008 two of the authors (FB and SE) decided to apply modern depth-sensing nanoindentation (DSNI) techniques to study mechanical properties of coal macerals and fine structure of coals. After preparation of very smooth samples of coals, the initial series of tests were performed by S. Bull (Newcastle University, UK). In 2010 a novel experimental procedure for DSNI studies of coals was presented at Newcastle nanoindentation conference. The procedure combined application of DSNI to very thin coal samples and the use of transmitted light microscopy (see [29]). At this presentation, the following drawbacks of microhardness tests were mentioned: (i) results obtained for relatively thick polished samples of coals depend on the presence of voids and microcracks and the inhomogeneity in-depth of a sample; (ii) the test results vary for the same sample, hence 10-30 measurements were usually taken to estimate the range of the values obtained; (iii) one cannot estimate the mechanical properties within the border region of two different macerals. In addition, although it is possible to evaluate microhardness of macerals of the vitrinite group in a reliable way, the microhardness indenters can barely be used to evaluate the microhardness of macerals of the inertinite group and they cannot be used for measurements of the properties of macerals of the liptinite group due to the small size of these maceral inclusions. Due to these drawbacks and scale issues, the results published on microhardness testing of distinct groups of macerals are not in full agreement with each other. The further results of DSNI tests obtained using this procedure and analysis of the experimental data were described in [30,31]. The DSI by microindenter was independently applied to coal samples in [32] using another procedure. More advanced micro and nanoindentation procedures and results of their applications to coals are presented in [33–35]. However, there are still many questions related to nanoindntation testing of coals.

The paper is organized as follows. First, we give some preliminary information concerning DSI and DSNI techniques. Then we discuss both Oliver-Pharr [36] and Galanov-Dub [37] approaches to extraction of mechanical properties from the indentation force-displacement curves.

Then we discuss possible experimental procedures for studying natural extreme materials. We discuss also the empirical and asymptotic approaches for studying characteristics of very thin samples glued to rigid substrate. These discussions are followed by presentation of new results on both micro/nanohardness tests and depth-sensing micro- and nanoindentation of samples of bituminous coal and anthracite. The scaling effects observed are described.

Finally, we argue that the values of the hardness obtained by microindenters and nanoindenters may be not compatible. In addition, we argue that analytical treatment of the DSI data employing either the Oliver-Pharr or the Galanov-Dub approaches may be meaningless in application to bituminous coals, while it may be reasonable in application to anthracite samples.

2 DSI and the Oliver-Pharr and the Galanov-Dub approaches

Depth-sensing indentation techniques were introduced by Kalei in his PhD thesis supervised by M.M. Khrushchov. In 1968 the first paper on DSI was published [38]. One can find reviews dedicated to development of hardness tests and depth-sensing indentation in [39–41]. If the depth of indentation is below micrometre scale, then the term DSNI is used. As a part of DSI, the $P-h$ diagram is continuously monitored for load increase and decrease, where, h is the depth of indentation (penetration of the indenter into the sample surface) and P is the force loading the indenter. In other words, the diagrams are recorded for loading and unloading of the indenter in the test samples in terms of "force-displacement" or "force-depth of indentation" coordinates. Typical $P-h$ curves for metals and many materials have usually two branches that do not coincide because the curve reflects both elastic and plastic deformation of the material at the loading, while the unloading of metals occurs usually elastically. Then in 1975 the Bulychev-Alekhin-Shorshorov (BASh) relation was derived [42]

$$S = dP/dh = 2E^* a \approx 2E^* \sqrt{A/\pi}, \tag{1}$$

where S is the inclination of the displacement-load curve, a is the characteristic size of the contact zone, A is the area of the contact and E^* is the reduced elastic modulus of the contact pair 'sample-indentor'. Within the framework of the Hertz contact theory, E^* is determined as a combination of elastic moduli E_i and E_s and Poisson's ratios ν_i and ν_s for indenter (with index i) and sample (index s):

$$\frac{1}{E^*} = \frac{1-\nu_i^2}{E_i} + \frac{1-\nu_s^2}{E_s}. \tag{2}$$

Although the use of the reduced elastic contact modulus for sharp indenters (or pointed indenters [40]) is not mathematically justified because the Hertz approximation of contacting solids as elastic half-spaces is violated in application to sharp indenters, currently (2) is employed in almost all models used by materials science community (see discussions in [40, 41]).

Thus, the basic relations for determination of the sample elastic modulus E_s and hardness HM are as follows:

$$E_s = \left(1 - \frac{E^*}{E_i^*}\right)^{-1} \left(1-\nu_s^2\right) E^*, \tag{3}$$

where ν_s is the sample Poisson's ratio, $E_i^* = \dfrac{E_i}{1-\nu_i^2}$ is the reduced elastic contact modulus of the indenter;

$$HM = \frac{P_{max}}{A}, \tag{4}$$

where P_{max} is the peak force applied to the surface by indenter.

The BASh relation (1) accompanied by additional assumptions allow calculation of local values of the reduced elastic contact modulus and hardness of the sample using either Oliver-Pharr [36] or Galanov-Dub [37] approaches.

Both approaches introduce relations between P and h of the unloading curve.

During the last few decades, the Oliver and Pharr (OP) approach for evaluation of elastic moduli and hardness of materials [36, 43] is generally included into the DSNI equipment software. The OP technique is based on the use of experimental values of the maximum load P_{max}, the corresponding maximum approach h_{max} of the indenter and sample, and values of the elastic stiffness S, measured for the unloading branch of the $P-h$ curve at $P = P_{max}$ and $h = h_{max}$. It is assumed that the contact surfaces of the indenter and flat sample after the deformation and the surface of the indenter itself are of the same type: spherical, if the indenter has a spherical surface; conical, if the indenter has a conical surface; pyramidal, if the indenter has a pyramidal surface; etc. Upon unloading, that is assumed to be elastic, the surfaces of the indenter and sample have the same property, i.e., they are surfaces of the same type as the indenter, and at the beginning of the repeated loading they touch at a single point.

However, the OP approach has been recently criticized [37, 41]. In particular, the OP approach does not consider the Galanov effect (the effective shape effect). Indeed, it was noted by Galanov and his co-workers as early as in 1983 [44, 45], that the real distance between the indenter and the surface of the imprint is not the same as the distance between a flat surface and the indenter. Hence, in analysis of the unloading branch of the $P-h$ curve, one has to take into account both the shift of the displacement axis due to a residual depth of plastic indentation and also the effective distance between the indenter and the imprint surface (the Galanov effect).

There were attempts to take into account the Galanov effect just by introducing into the BASh relation a correction factor β for the indenter shape, i.e. to write (1) as $S \approx 2\beta E^* \sqrt{A/\pi}$ (see a discussion in [44]). However, an introduction of such a factor does not save the situation. Galanov and Dub [37] argued that the main assumptions of the OP approach are violated and therefore, the various correction factors are introduced without proper theoretical justification [43]. The most important is that the depth of indentation is not estimated properly. This causes the systematic mistakes in measuring hardness (up to 10%) and elastic moduli of materials (up to 15%) which were noticed by experimenters [46–51]. There were attempts to take into account the elastic deformations of the indenters [46–51], imperfection of their geometry, and other factors [36, 43]. Further critique of the OP approach has been recently presented by Chaudhri [41].

Let us describe briefly the main point of the Galanov-Dub (GD) approach that may be considered as a refinement of the BASh and OP techniques. For the sake of simplicity, the formulae are presented only for a conical indenter. The full derivation of the formulae can be found in [37]. It should be mentioned that the Galanov-Dub approach was derived without additional assump-

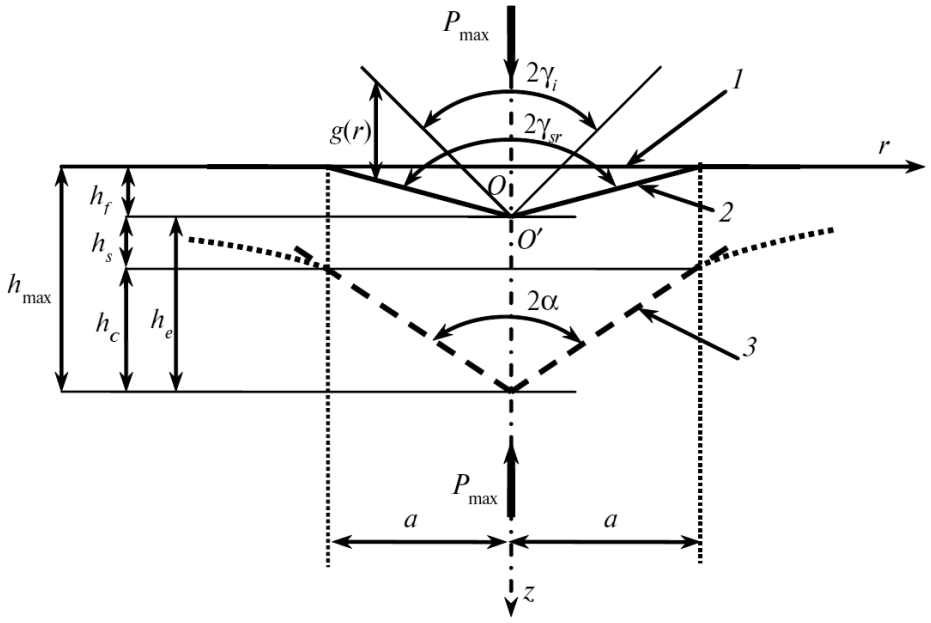

Fig. 1 Scheme of elastic contact between a conical indenter and a conical imprint (2) in the sample (1). The initial surface of the sample $z = 0$; the apex angle of the surface of the imprint is $2\gamma_{sr}$; the form of equivalent conical indenter (3) is described as $g(r) = r^2 \cot\alpha$.

tions to ones used by the OP method and additional experimental measurements.

Let us consider a conical indenter with the apex angle $2\gamma_i$ using the cylindrical coordinate system $Or\phi z$. The sample-rigid conical indenter scheme in the presence of the Galanov effect [44] is shown in Figure 1. Note that in Figure 1 all dimensions of the scheme are rather distorted. This scheme is the basis for the GD method [37]. The indenter contacts with a conical imprint with the apex angle $2\gamma_{sr}$. The effective distance between the surfaces is described by the function $g(r) = r^2 \cot\alpha$, where α is the effective cone apex semi-angle. OO' is the shift of the displacement origin. The following values are shown

$$h_c = \frac{4}{\pi}\frac{P_{max}}{S},\ h_s = \frac{2(\pi-2)}{\pi}\frac{P_{max}}{S},$$

$$h_e = (h_{max} - h_f) = \frac{2P_{max}}{S},$$

$$\cot\alpha = \cot\gamma_i - \cot\gamma_{sr}.$$

Note that h_c is the nominal contact depth [37] here, and it is not equal to contact depth h_c of [36, 43].

A transition from conical to equivalent pyramidal or spherical indenters may be implemented assuming the equality of the projections areas of imprints made by different indenters at the same volume of penetration (the same penetration depths for pyramidal and conical indenters). This condition leads to the following relation between the apex angles of equivalent conical, pyramidal (trihedral and tetrahedral) and spherical indenters:

$$\cot\gamma_i = \frac{\sqrt{\pi}}{2}\cot\gamma_V = \sqrt[4]{\frac{\pi^2}{27}}\cot\gamma_B = \frac{3}{4}\frac{a}{R}, \qquad (5)$$

where γ_i, γ_V, γ_B are apex angles of indenters: conical γ_i, tetrahedral (e.g., Vickers, $\gamma_V = 68°$) and trihedral (e.g.,

Berkovich, $\gamma_B = 65°$), respectively; a/R is the ratio of the imprint radius to the radius of the spherical indenter.

The GD method takes into account the elastic deformations of the indenter and sample in the determination of the contact area and use the same experimental values of the $P - h$ diagram (see Figure 2). The characteristic scale parameters of small forces P_c and displacements δ_c mentioned in Figure 2 are closely connected with both the specific work of the adhesion (w) and reduced contact modulus E^* of the contacting pair 'sample-indentor' [52], as well as the indentor shape. For example, in case when the indentor has the conical shape with the apex angle of $2\gamma_i$, the corresponding scale parameters could be calculated as follows [37]

$$P_c = \frac{54w^2}{\pi E^* \cot^3 \gamma_i}, \quad \delta_c = \frac{w}{E^* \cot \gamma_i}.$$

These quantities give an evaluation of the scales of forces and displacements at which the adhesion forces effect may be considerable in terms of interpretation of the DSI data.

Derivation of relation for the hardness HM of the material is based on the accepted hypotheses the area of the recovered imprint projection onto the $z = 0$ plane (Figure 2)

$$A = F(h_f),\ F(h_f) = \pi a^2 = \pi h_f^2 \tan^2 \gamma_{sr}. \qquad (6)$$

From (6) and from the determination of Meyer, hardness HM and equality $\cot \gamma_{sr} = \cot \gamma_i - \dfrac{2HM}{E^*}$ [53], we derive a square equation for HM

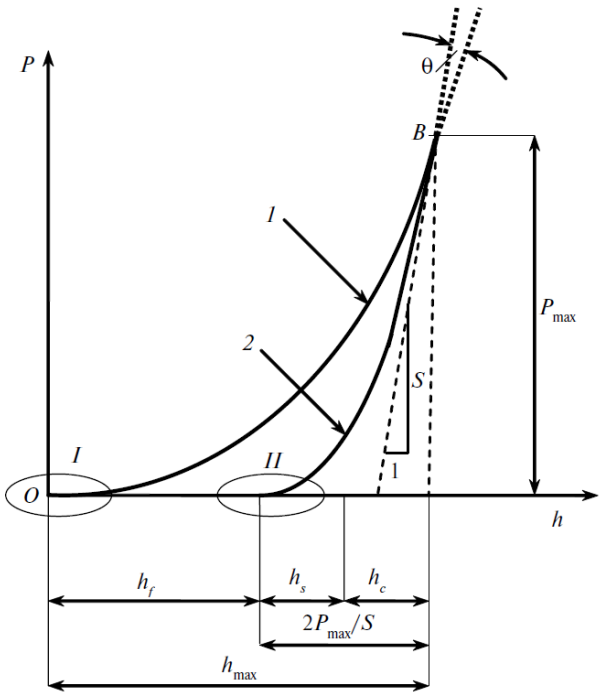

Fig. 2 Scheme of the dependence $P(h)$: regions of loading (1) and unloading (2) of the indenter; I - the region of small values $P \sim P_c$ and $h \sim \delta_c$ (see Figure 1), II - the region of small values $P \sim P_c$ and $(h \sim h_f) \sim \delta_c$; P_c and δ_c are characteristic scales of small forces P and displacements h (after [37]).

$$HM = \frac{P_{max}}{A} = \frac{P_{max}}{\pi h_f^2} \cot^2 \gamma_{sr} = \\ = \frac{P_{max}}{\pi h_f^2} \left(\cot \gamma_i - \frac{2HM}{E^*} \right)^2, \qquad (7)$$

where $h_f = h_{max} - \dfrac{2P_{max}}{S}$. After some mathematical procedures one may arrive at the following formulae for calculating of hardness by experimental data:

$$HM = \chi \frac{P_{max} \cot^2 \gamma_i}{\pi h_f^2};\ h_f = h_{max} - \frac{2P_{max}}{S} \\ \chi = \frac{4}{\left(\sqrt{1 + 4\beta \cot \gamma_i} + 1 \right)^2} \leqslant 1;\ \beta = \frac{2P_{max}}{\pi h_f^2 E^*}, \qquad (8)$$

where coefficient $\chi = \dfrac{4}{\left(\sqrt{1 + 4\beta \cot \gamma_i} + 1 \right)^2} \leqslant 1$ allows for the elastic deformation of the indenter and sample.

The following formulas for HM are equivalent by accuracy

$$HM = \frac{4}{\pi}\frac{P_{max}E^{*2}}{S^2}, \quad (9)$$

$$HM = \frac{b\cot\gamma_i}{2(b+1)}E^*;\ b = \frac{2}{\pi}\left(\frac{h_{max}S}{2P_{max}} - 1\right)^{-1}. \quad (10)$$

Note that all the equivalent relations (8)-(10) for hardness calculations are strongly dependent on two values, namely, reduced elastic modulus E^* and contact stiffness S, such that HM is defined after determination of E^* and S.

Derivation of formula for determination of the value of reduced elastic modulus E^* is based on the following theoretical relation obtained using solution of the elastic contact problem during the cone indentation into a conical imprint [54].

$$\begin{aligned} &P = \frac{2E^*}{\pi\left(\cot\gamma_i - \cot\gamma_{sr}\right)}\left(h - h_f\right), \\ &\cot\gamma_{sr} = \cot\gamma_i - \frac{2HM}{E^*},\ h_f = h_{max} - \frac{2P_{max}}{S}. \end{aligned} \quad (11)$$

After the transformations, it takes the form

$$P = \frac{E^{*2}}{\pi HM}\left(h - h_f\right)^2.$$

From here, taking into account that $HM = P_{max}/A$ at $h = h_{max}$ and $P = P_{max}$, we have the known relation (1).

Again, using the above relations and known formula for hardness, we arrive at formulae for the determination of effective (reduced) elastic modulus E^*

$$\begin{aligned} &E^* = \frac{2P_{max}\cot\gamma_i}{\pi h_f^2\xi^*},\ h_f = h_{max} - \frac{2P_{max}}{S}, \\ &\xi^* = b(1+b),\ b = \frac{2}{\pi}\left(\frac{h_{max}S}{2P_{max}} - 1\right)^{-1}, \\ &E_s = \left(1 - \frac{E^*}{E_i^*}\right)^{-1}(1-\nu_s^2)E^*, \end{aligned} \quad (12)$$

or equivalent ones as

$$E^* = \frac{\pi}{8}\frac{b\cot\gamma_i}{(b+1)}\frac{S^2}{P_{max}},\ b = \frac{2}{\pi}\left(\frac{h_{max}S}{2P_{max}} - 1\right)^{-1}. \quad (13)$$

For the determination of stiffness S involved in E^* and HM, the new procedure is proposed which is based on the hypothesis of the elastic unloading of the contact pair sample-indenter after applying forces $P = P_{max}$, which activates the sufficiently developed plastic deformation (it should be recalled that the total procedure of the determination of the hardness and elastic moduli presented in contrast with [36, 43] is based on this hypothesis). Taking *a priori* this hypothesis, the unloading branch (see Figure 2) may be presented by the following precise functional relation:

$$\begin{aligned} &P = \frac{S^2}{4P_{max}}\left(h - h_{max} + \frac{2P_{max}}{S}\right)^2, \\ &\frac{dP}{dh} = \frac{S^2}{2P_{max}}\left(h - h_{max} + \frac{2P_{max}}{S}\right), \\ &\left.\frac{dP}{dh}\right|_{h=h_{max}} = S, \end{aligned} \quad (14)$$

which is based only on experimentally measured values P_{max}, h_{max} and S and the assumption of elastic unloading.

The determination of stiffness $S = \left.\frac{dP}{dh}\right|_{h=h_{max}}$ using the experimental values of the function $P(h)$ for the unloading branch is, generally, mathematically ill-posed problem of the differentiation of experimental data that is unstable with respect to their small disturbances. However, the use of an expression of the form (14) permits to define the stable value S.

It is assumed in Eq. (14) that the P_{max}, h_{max} values are measured sufficiently accurate and they are known,

while the S value is unknown. To determine this value from Eq. (14), we have the following overdetermined system of quadratic equations:

$$\begin{aligned} &(1-\delta_i S)^2 - \overline{P}_i = 0,\ \delta_i = \frac{h_{max}-h_i}{2P_{max}} \geqslant 0, \\ &\overline{P}_i = \frac{P_i}{P_{max}},\ i = 1,2,3,...,N, \end{aligned} \tag{15}$$

where h_i, $P_i = P(h_i)$, $i = 1,2,3,...,N$ are experimental quantities, which are coordinates of the points of the unloading curve (see Figure 2). In calculations of these experimental quantities are convenient to note in order of increasing or decreasing. The system (15) is equivalent to the overspecified system of linear equations

$$\begin{aligned} &(1-\delta_i S) - \sqrt{\overline{P}_i} = 0,\ \delta_i = \frac{h_{max}-h_i}{2P_{max}} \geqslant 0, \\ &\overline{P}_i = \frac{P_i}{P_{max}},\ i = 1,2,3,...,N, \end{aligned} \tag{16}$$

which has a unique stable normal pseudo-solution (solution) [55–57]:

$$\begin{aligned} &S = \frac{\sum\limits_{i=1}^{N} \delta_i \left(1 - \sqrt{\overline{P}_i}\right)}{\sum\limits_{i=1}^{N} \delta_i^2} > 0, \\ &\sum_{i=1}^{N} \delta_i^2 \neq 0,\ \delta_i = \frac{h_{max}-h_i}{2P_{max}} \geqslant 0,\ \overline{P}_i = \frac{P_i}{P_{max}}, \end{aligned} \tag{17}$$

i.e., it is the best approximate (generalized) solution to the system (15), and it has the least stiffness S and minimizes the discrepancy r for equations (16)

$$r^2 = \sum_{i=1}^{N} \left((1-\delta_i S) - \sqrt{\overline{P}_i} \right)^2.$$

Finally, the solution for stiffness S has form of (17), where h_i, $P_i = P(h_i)$, $i = 1,2,3,...,N$ are experimental quantities, which are coordinates of the points of the unloading curve of the $P-h$ diagram (see Figure 2).

3 Preparation of samples for DSI and Microhardness Tests

The common procedures of nanoindentation could not be used directly for the investigation of components of a spatially inhomogeneous materials as rocks, bones and coals. To apply DSI techniques to coals, one needs to prepare proper samples and design the sequence of the experimental procedures. Then proper analysis of the data should be used.

To explain the specific difficulties in DSI testing of coals, let us compare them with another class of extreme natural materials as bones. Both classes of materials (coals and bones) are heterogeneous, hierarchical composite materials with important structural features spanning multiple length scales; both classes of materials contain multiple pores. In addition, both classes have internal layered anisotropic structures and the anisotropy that depends on the length scale of consideration [3, 30, 58–61]. Recently a series of papers devoted to DSNI analysis of various biomaterials was published by P. Vena (Politecnico di Milano) and his co-workers [61–63]. In particular, they studied adult bovine cortical bones. The nanoindentation tests of bones were performed on the same osteonal structure in the axial (along the long bone axis) and transverse (perpendicular to the long bone axis) directions. The indents were located along arrays going radially out from the Haversian canal. The maximum depths of the indents (50, 100, 200 and 300 nm)

differ from one radial direction to another one. A special cubic sample holder was made that could keep the polished sample at its corner. This design allowed the researchers to perform mechanical test of the same osteon in both axial and transverse directions [61] and analyse their mechanical properties using the OP approach. It was found that the hierarchical arrangement of lamellar bone is the major determinant for modulation of mechanical properties and anisotropic mechanical behaviour of the tissue. Because coals are normally very brittle, it was impossible to prepare cubic samples with polished sides. Hence, the procedures used for the DSNI studies of bones are not applicable directly to coals.

Alternatively, it was proposed [29] to apply the DSNI to very thin films of the tested coal samples (the thickness is about 10-20 μm) glued to a transparent rigid substrate. The combination of DSNI and transmitted light microscopy allowed to visualize the regions of tested maceral components [29].

After DSI tests of a thin sample that is attached to an elastic substrate, one extracts as E^* not the modulus of the sample but rather an equivalent modulus (E^*_{eq}) of the system sample-substrate. Because we study not a bulk material, but rather thin films glued to the substrate, the approximating functions were used to extract the real elastic modulus of the tested component [31]. The relations among the equivalent modulus, the contact moduli of substrate (glue) E^*_s and the sample (film) E^*_f may be expressed as [31, 64]

$$E^*_{eq} = E^*_s + \left(E^*_f - E^*_s\right) \Phi(x), \tag{18}$$

where $\Phi(x)$ is a weight function of relative penetration depth x. This function tends to zero at very high depth values and $\Phi(0) = 1$. For Vickers or Berkovich pyramidal indenters, the relative penetration depth may be estimated as $x = a/t \approx \sqrt{24.5/\pi} \cdot h/t$, where t is the film thickness. Comparing the experimental values with the results of approximations and calculating statistical characteristics, the most appropriate approximate functions were found. The further studies [58] showed that these functions disagree with the analytical fitting function obtained by the asymptotic approach. On the other hand, the asymptotical approximations are in good agreement with experimental results on DSNI of thin ductile layers of metals. This disagreement was explained by the presence of structural transformations of the coals during loading. Indeed, at unloading of a brittle coal sample, its material within the indentation zone is no longer a continuous elastic medium but rather a fine powder of crushed material.

The above procedure of application of the combination of DSNI and transmitted light optical microscopy [29] was applied to coal samples whose thickness was around 13-14 microns [30, 31]. In fact, two types of microscopes were employed. Microscope operating in transmitted light was used to allocate the coordinates of a specific components of the coal sample, i.e. the indenta-

tion was in the domains occupied by the clearly visible maceral, and to prescribe the path of the indenter movement on the motorized table of automated depth-sensing nanoindentation system; while accuracy in setting the area of the indentation was confirmed by microscope, operating in reflected light. It was argued that the use of very thin petrographic sections has several advantages. In particular, it was possible to assume confidently that the components of the material are presented along the entire thickness of the sample and the effects of pores and cracks during the indentation are practically removed. In addition, thin coal films are transparent, therefore may be used for experiments with microscopes operating in transmitted light. Using the above described procedure employing thin films of coals, mechanical properties of lignites were studied at nanoscale [34]. These studies revealed changes in vitrinite mechanical properties with coal type and rank, while values of mechanical properties of inertinites did not vary practically for all lignite and bituminous (hard) coals.

On the other hand, the above-mentioned procedure has some drawbacks. Indeed, the relatively thin coal samples were impregnated in order to harden the interporous walls, while this could affect the results. It was difficult to study anisotropy of the materials. The anthracite samples whose thickness was just 10 μm, were not transparent. Hence, another procedure of preparation of the coal samples was also used for the DSI experiments [33]. Namely, samples were manufactured from fragments of coal and anthracite whose thickness was not smaller than 20-30 mm. No binders or cementing admixtures, or mechanical compaction were involved at any stage of preparation. The samples surfaces selected for further indentation experiments were smoothed and polished using polishing machine RotoPol-35 (Struers, Demark). Final smoothing (polishing) was carried out with glycerine instead of water. The resultant samples had comparable dimension with the sizes of the initial fragments, with height of 10-25 mm. The surface prepared to indentation tests was oriented perpendicular to the bedding direction.

Instrumented tests were performed at two different DSI facilities: nanotriboindenter Hysitron TI750 UBI with Berkovich indenter and MicroHardness Tester (CSM Instruments) with Vickers indenter. The latter allows tests at relatively higher peak loads (up to 1000mN), whereas the P_{max} of the former device is limited to 12 mN. Additionally, hardness measurements were performed at PMT-3 microhardness tester (LOMO, Russia). It is worthwhile to note that the PMT-3 device does not provide the continuous monitoring of the $P-h$ curve but rather allowed us to measure the hardness after the unloading of the sample. Hence, the microhardness tests are referred to as static microindentation tests.

Experiments at Hysitron TI750 UBI were done by load-control mode with trapezoidal protocol (two seconds hold at peak load). At each sample, first, a maceral of interest was identified. Then according to the limita-

Table 1 Characteristics of the tested coal and anthracite samples

#	Type	Maceral composition, % vol.			Vitrinite reflectance index, $R_{O,r}$,% vol.	Carbon, C^{daf}, % (on dry, ash-free basis)
		Vitrinite Vt	Inertinite I	Liptinite L		
1	low-rank bituminous coal	70.0	20.0	10.0	0.65	80.19
2	anthracite	91.0	9.0	0.0	3.58	92.39

tions of the technique of Hysitron TI750 UBI device, a square 70×70 μm area was chosen and series of DSI measurements (not less than 36 indents) were implemented within this area. Tests at MicroHardness Tester were also done using load-control mode with trapezoidal protocol with 15s hold at maximum load. Microhardness measurements at PMT-3 were done with 10s hold at load.

In this work we primarily concentrated on coals of two types: a low-rank bituminous coal (type # 1) and anthracite (type # 2). The main structural characteristics are listed in Table 1. It is worth to note that the maceral composition of anthracite cannot be determined just by the use of optical microscopy and rather complicated techniques have to be used. In fact, anthracitization of coals is accompanied by a clustering of graphene domains (carbon perfect aromatic lamellae), which results in a rapid increase of sizes of the graphene components and porosity [3].

For indentations of the vitrinite maceral domains of the coal #1, the peak load P_{max} were as follows: 4 mN for DSNI, 500 mN for DSI by the microindenter, and 200, 500 and 1000 mN for microhardness measurements. At each sample, not less than 15 indentations were performed for the vitrinite maceral domains.

In addition, the coal sample #2 (anthracite) and the inertinite domains of the coal #1 were also tested. The loading modes were similar to the described above, however the peak load values differ slightly. The values of P_{max} were as follows: 10 mN for DSNI tests and 500 mN for DSI test using microindenter.

4 Micro and nanoindentation tests for evaluation of hardness and elastic moduli of vitrinite

Here the results of evaluation of hardness and elastic moduli of coals are presented. First, the hardness of vitrinite maceral of the coal #1 is calculated according to standards [15, 28], while the elastic contact modulus is evaluated according to standard OP approach [36]. Then the same characteristics are evaluated according to the refined GD approach.

4.1 Results of applications of standard procedures of hardness and elastic moduli evaluations

The typical imprints obtained for the coal #1 after hardness measurements tests at different loads are shown in Figure 3. One can see that the sizes of the imprints increase drastically with growth of the maximum indentation force. Indeed, the average values of the measured diagonals ($d_{average}$) are: $d_{average} = 30$ μm for $P_{max} = 200$ mN, $d_{average} = 50$ μm for $P_{max} = 500$ mN, and $d_{average} = 78$ μm at $P_{max} = 1000$ mN.

One can also observe cracks within the imprints and an external crack coming out of the edge of one diagonal in the case when $P_{max} = 1000$ mN.

Let us describe now the results of evaluation of elastic moduli and values of hardness at different scales. For vitrinite maceral domains of the coal #1, Table 2 shows the elastic moduli extracted from the DSI tests using the OP approach and values of hardness that were found by static indentation at PMT-3 device.

It could be seen from Table 2 that the values of elastic moduli measured at different scales of indentation are very similar. On the other hand, the hardness values decrease with growth of the peak load, as shown in Figure 4. It should be especially pointed out that the correlation between these quantities is rather good. It can be quantitatively characterized by the coefficient of determination R^2 [65]. One can observe an unexpectedly fast decay of hardness values with the increase of the peak load acting on the indenter, whereas elastic moduli are rather similar for both scales of indentation.

To evaluate the elastic contact modulus, one needs to analyse the experimental load-displacement curves. Figure 5 demonstrates the typical shapes of $P - h$ curves obtained at nano- and microindentation of the coal #1. As it has been observed for other coals [35], the shapes of load-displacement diagrams obtained after nano- and microindentation are qualitatively similar. To characterize such a similarity quantitatively, we use a parameter (R_W, %) that is the ratio between the hysteresis loop (A_{hys}) to the full work of indenter tip at loading of the sample (A_{load}). Therefore, parameter R_W is calculated as follows:

$$R_W = \frac{A_{hys}}{A_{load}} \cdot 100\%. \tag{19}$$

A scheme explaining the meaning of A_{hys} and A_{load} works is shown in Figure 6.

The average values of R_W for the coal #1 at nanoindentation were $R_W = 34.2 \pm 1.5\%$, whereas at microindentation $R_W = 36.0 \pm 2.0\%$, and these could be considered as similar for both nano and microscales of tests.

One could expect that the values of hardness obtained in static experiments by the microhardness device should be higher than the values obtained in DSNI tests because the area used in (4) is the elastically recovered area of the imprint after full unloading, while one uses in a DSNI test the area of the contact region under maximum load. However, we obtained the opposite result. Despite the fact that, at nanoindentation tests, the

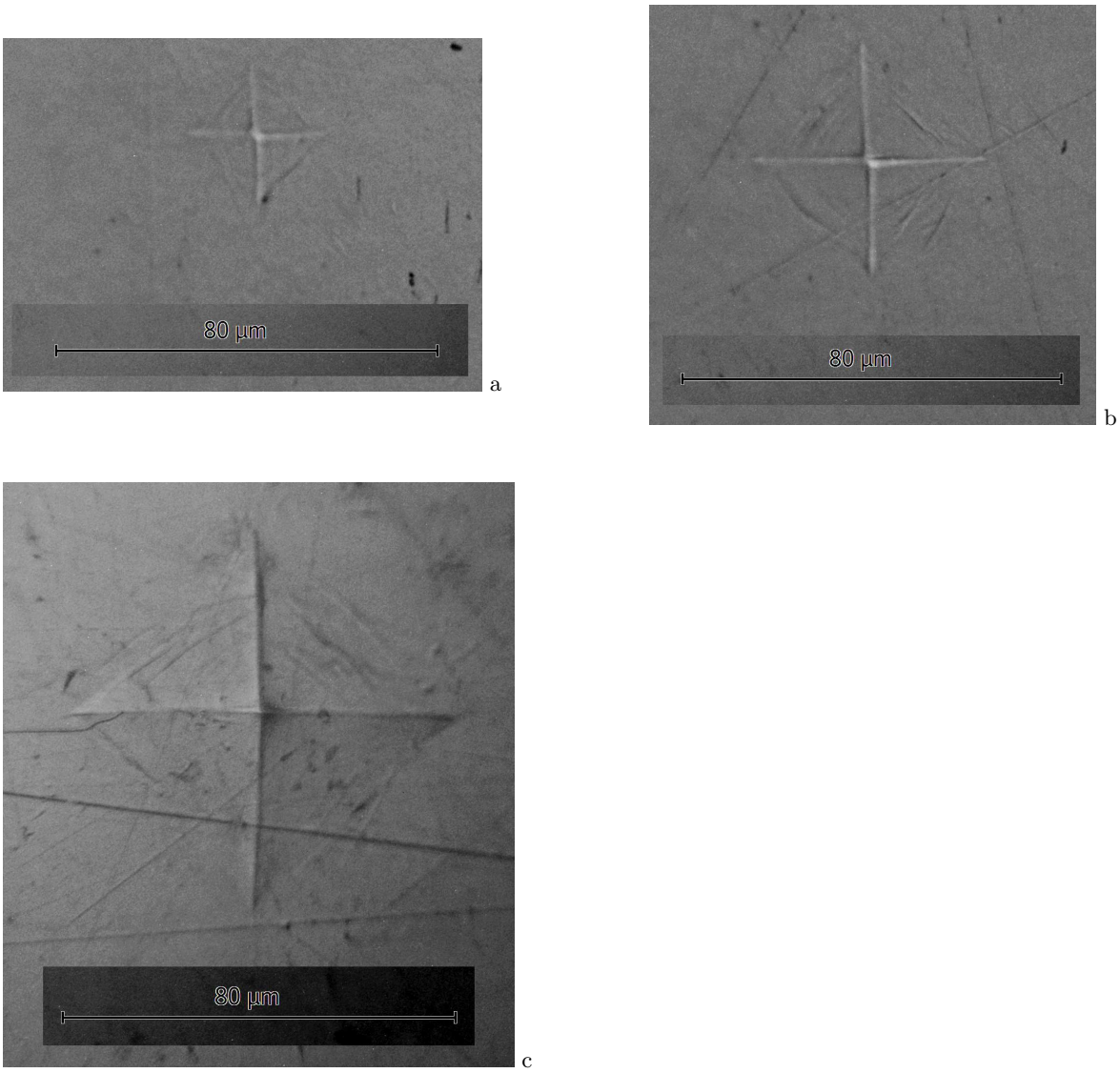

Fig. 3 Typical shapes of imprints obtained in static microhardness tests of the bituminous coal #1 at different peak loads: a) P_{max} = 200 mN; b) P_{max} = 500 mN; c) P_{max} = 1000 mN.

results are quite 'stable' (see HM standard deviations shown in Table 2 line 'DSI, nanoindentation'), the hardness at nanoscale is relatively higher than the hardness found by microhardness DSI and static tests. Also, it should be mentioned that the average values of hardness measured by DSI and static indentation are similar, but the standard deviation of HM (as of DSI) is rather high in comparison to the one related to static technique.

4.2 Hardness and elastic moduli evaluations using the GD approach

On the basis of the relations presented in section 3, evaluations of elastic moduli and hardness for the coal #1 (for DSI techniques only) were made and compared to the ones shown in Table 2. In addition, the following distinctions in approaches were calculated in accordance

Table 2 Values of elastic moduli and hardness of the coal #1 within a vitrinite maceral domain measured at different peak loads.

Type of indentation (DSI or static, nano or micro)	Peak load P_{max}, mN	Elastic modulus of E_s^{OP}, GPa (average)	Standard deviation E_s^{OP}, GPa	Hardness HM, MPa (average)	Standard deviation of HM, MPa
DSI, nano	4	3.60	0.08	469.75	1.18
Static, micro	200	-	-	403.63	15.63
DSI, micro	500	3.62	0.07	388.71	37.46
Static, micro	500	-	-	367.01	4.37
Static, micro	1000	-	-	299.90	3.68

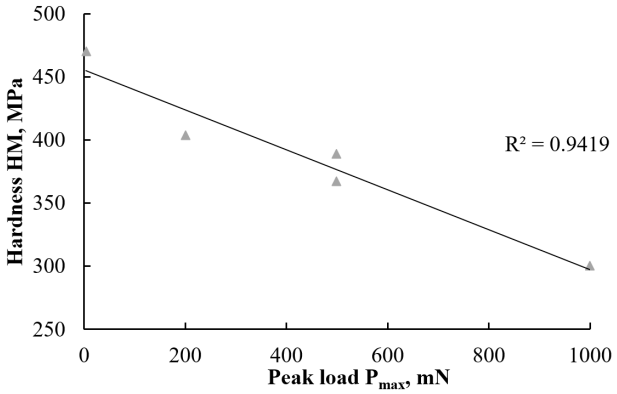

Fig. 4 Scaling effects of the hardness values for the coal #1. The hardness values are calculated according to the OP approach. R^2 is the coefficient of determination.

with relations (20)

$$\varepsilon^E_{OPGD} = \frac{E_s^{GD} - E_s^{OP}}{E_s^{OP}}, \qquad \varepsilon^H_{OPGD} = \frac{HM^{GD} - HM^{OP}}{HM^{OP}}, \tag{20}$$

where E_s^{OP}, E_s^{OP} are elastic moduli measured by OP and GD techniques, HM^{OP}, HM^{GD} are corresponding hardness values. The results are shown in Table 3.

One can see that the values of moduli extracted by the GD method are systematically higher than the values obtained by the OP method, while the opposite results are obtained for values of hardness extracted by the use of these two approaches. One of possible explanations is that values of hardness in the GD approach are calculated using not only the slope S at point , i.e. (h_{max}, P_{max}) but also the elastically recovered area of imprint (see (6) and Figure 2) that is larger than the current contact area used in the OP approach.

It should be mentioned that the GD approach allowed revealing differences between the measured elastic moduli at micro- and nanoindentation. The growth of E_s for the large loads may be explained that the coal internal structure is crashed within a small zone under the indenter tip.

Further, the GD technique allowed reduction of the standard deviation values for both elastic moduli and hardness. Moreover, the hardness value obtained at peak load of 500mN now is much more similar to the one

Table 3 Values of elastic moduli and hardness of the coal #1 measured by the GD approach.

Type of indentation (micro or nanoindentation)	Peak load P_{max}, mN	Elastic modulus E_s^{GD}, GPa (average)	Standard deviation of E_s^{GD}, GPa	ε^E_{OPGD}, %	Hardness HM^{GD}, MPa (average)	Standard deviation of HM^{GD}, MPa	ε^H_{OPGD}, %
nanoindentation	4	3.68	0.06	1.53	451.11	1.14	-3.97
microindentation	500	4.34	0.10	19.88	360.15	1.21	-7.35

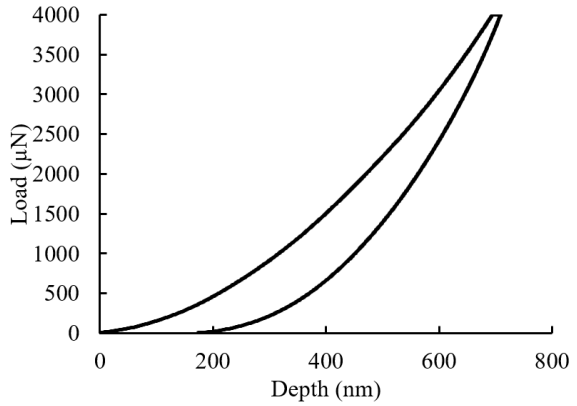

a

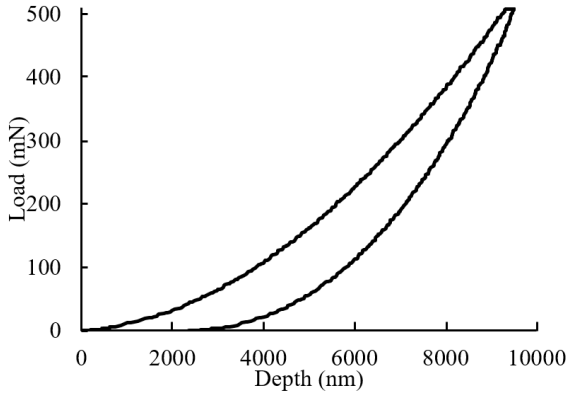

b

Fig. 5 Typical load-displacement curves obtained for the coal #1 at a) nano- ; and b) micro scales of indentation.

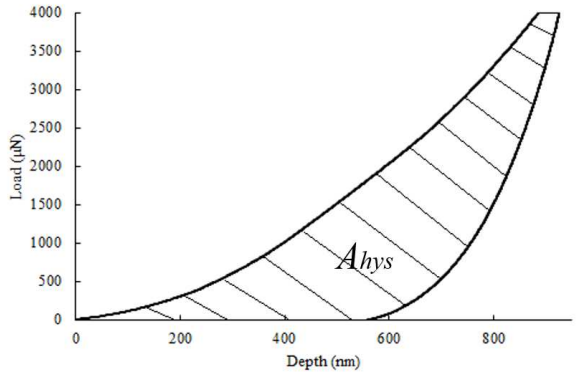

a

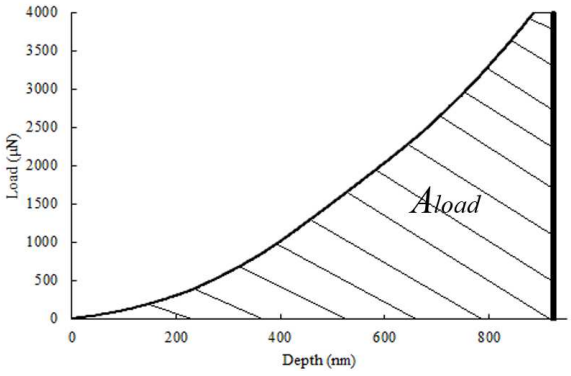

b

Fig. 6 The force-displacement curve and a scheme for evaluation of the components of R_W ratio. The works a) the A_{hys} and b) the A_{load} correspond to shaded areas of the graphs.

measured by the static indentation at the same force. In accordance with the GD measured values, correlation shown in Figure 6 transforms into the one presented in Figure 7.

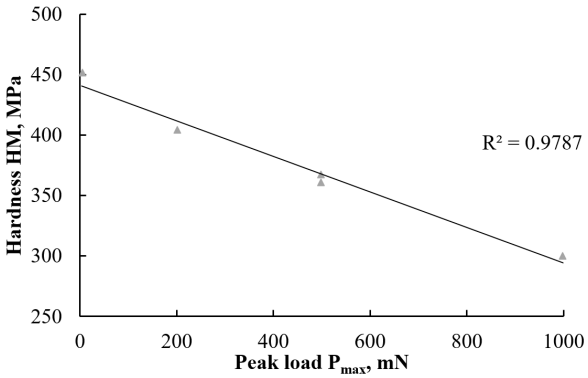

Fig. 7 Scaling effects of the hardness values for the coal #1 calculated according to the GD approach. R^2 is the coefficient of determination [65].

It could be seen that the hardness values decrease with growth of the peak load and this trend remains similar to the one shown in Figure 4, but the correlation coefficient has become even better.

The trends shown in Figures 4 and 7 could be explained by the fact that coal matter is being crushed into the fine powder in the contact zone between the surface of the sample and indenter tip. Hence, the hardness HM as constant value (independent of load) become meaningless.

4.3 Results for inertinite maceral of the bituminous coal #1 *and anthracite* #2

As it was mentioned previously, we investigated additionally the inertinite maceral of the coal #1 and anthracite #2.

Figure 8 shows comparison of the typical load-displacement diagrams obtained at different loading scales, for inertinite of the coal #1.

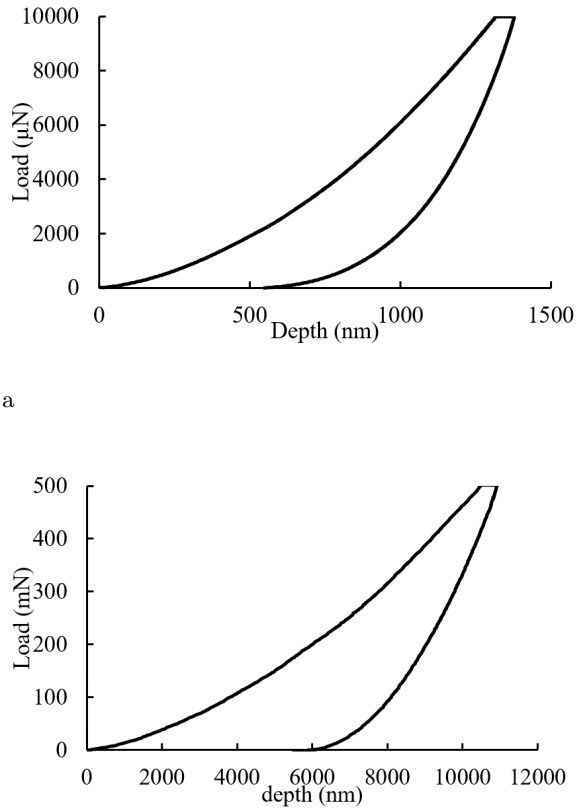

Fig. 8 Typical load-displacement curves obtained at the coal #1 (inertinite maceral) at a) nano-; and b) micro-scales of indentation.

It is obvious that again the curves are rather similar to each other. However, for this maceral, the parameter R_W is slightly larger in case of microindentation in comparison to nanoindentation, namely $R_W = 41.0 \pm 1.3\%$ for nanoindentation and $R_W = 45.3 \pm 1.0\%$ for microindentation.

Results of measurement of elastic moduli and hardness values of inertinite maceral of the coal #1 by both the OP and GD techniques are shown in Table 4.

It could be seen from Table 4 that for the inertinite maceral of the coal #1, the previous observation that

Table 4 Values of elastic moduli and hardness of the inertinite maceral of the coal #1 measured by the OP and GD approaches

P_{max}, mN	E_s^{OP}, GPa	St.Dev. E_s^{OP}, GPa	E_s^{GD} GPa	St.Dev. E_s^{GD}, GPa	ε^E_{OPGD}, %	HM^{OP}, MPa	St.Dev. HM^{OP}, MPa	HM^{GD}, MPa	St.Dev. HM^{GD}, MPa	ε^E_{OPGD}, %
10	5.13	0.34	5.61	0.14	9.38	463.62	58.71	421.72	50.50	-9.04
500	3.02	0.40	4.04	0.19	33.96	251.70	40.61	216.99	28.74	-13.79

the GD approach leads to increase of the elastic moduli values and decrease of values of hardness is still valid. In general, the values of both hardness and elastic modulus decrease with increase of the peak load regardless of the approach for their evaluation.

Let us now report the results obtained for anthracite. Figure 9 reveals comparison between typical load-displacemer curves for anthracite at nano and microscales of the maximum applied load.

One can see that both values of P_{max} are not large enough to create considerable imprint in the anthracite sample. The resulting images of the imprints (or lack of them) are shown in Figure 10. Nevertheless, the loading and unloading branches have distinctions. As it was expected, these diagrams are very similar for both scales of indentation. Parameter $R_W = 8.2 \pm 1.4\%$ for nanoindentation and $R_W = 10.8 \pm 0.7\%$ for microindentation. Although the hysteresis loop at microindentation is slightly wider than at nanoindentation, both R_W values are relatively small.

Results of measurement of elastic moduli and hardness values of anthracite (the coal #2) by both the OP and GD techniques are shown in Table 5.

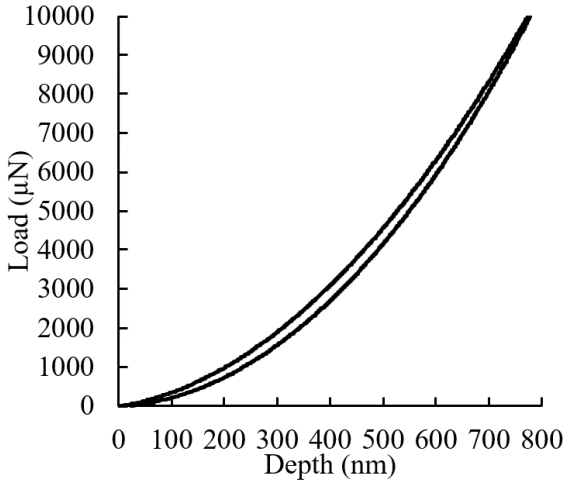

a

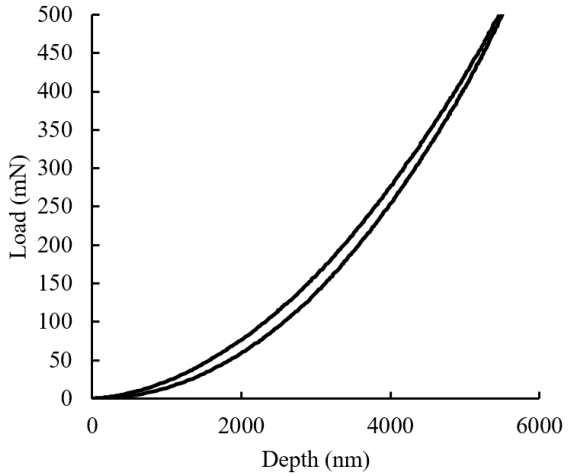

b

Fig. 9 Typical load-displacement curves obtained at anthracite #2 at different scales of indentation: a) nano-; b) micro.

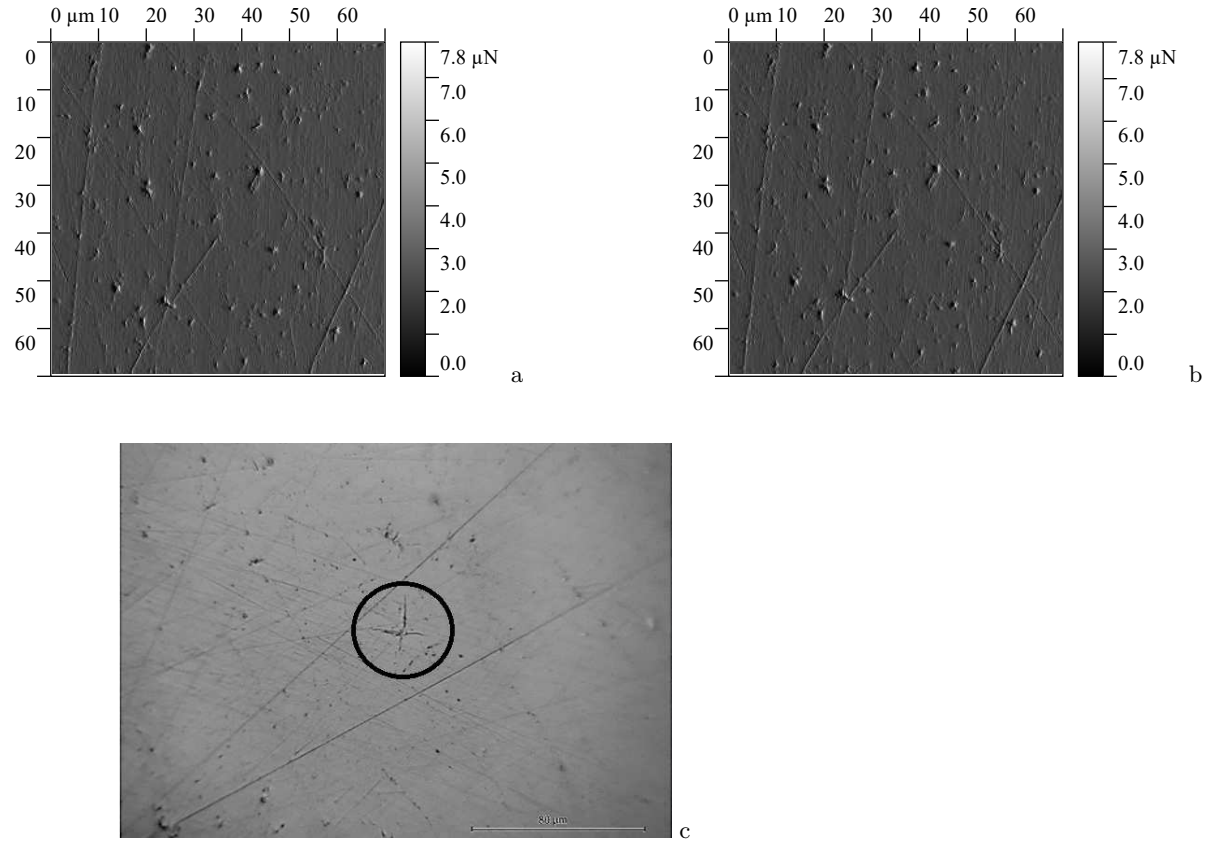

Fig. 10 Typical shapes of imprints obtained in static microhardness tests of the anthracite #2 at different peak loads: a) scanning probe microscopy image of the selected surface before DSNI tests; b) scanning probe microscopy image after DSNI at the specified area (P_{max} = 10 mN); c) optical microscopy image of the imprint after DSI microindentation (P_{max} = 500 mN). The contact area with the Vickers indentor is contained inside the black circle. Only surface damages could be observed at the contact of anthracite with sharp edges of the indentor tip. Comparison of a) and b) images reveals that there are no remaining imprints after a series of DSNI tests (here, total of 36 indents).

Table 5 Values of elastic moduli and hardness of anthracite #2 measured by the OP and GD approaches

P_{max}, mN	E_s^{OP}, GPa	St.Dev. E_s^{OP}, GPa	E_s^{GD} GPa	St.Dev. E_s^{GD}, GPa	ε^E_{OPGD}, %	HM^{OP}, MPa	St.Dev. HM^{OP}, MPa	HM^{GD}, MPa	St.Dev. HM^{GD}, MPa	ε^E_{OPGD}, %
10	9.29	0.18	9.00	0.11	-3.19	1687.55	62.02	1751.90	58.61	3.81
500	8.60	0.03	9.35	0.03	8.73	1641.76	24.85	1409.95	20.60	-14.12

It could be seen from Table 5 that there exists a disagreement with the previous observations that the GD approach leads to increase of the elastic moduli values and decrease of hardness in comparison with OP method. Namely, in case of nanoindentation, the elastic modulus decreased, whereas the hardness value slightly grew.

A possible explanation is the following. Both OP and GD approaches are dealing with the point $B(h_{max}, P_{max})$ on the $P-h$ diagram. If the load is very small ($P_{max} =$ 10mN), then the irreversible deformations are rather small, while the elastic recovery is almost full. Therefore, the main assumption of the GD approach is violated.

5 Conclusions

Coals are heterogeneous, hierarchical composite materials whose internal structural features spanning multiple length scales. Mechanical behaviour of coals was investigated using both static and depth-sensing indentation (DSI) techniques. The studies have been focused on low-rank bituminous coals and anthracite. Both nanoindentation and microindentation devices were employed. For analysis of the force-displacement curves obtained by DSI, both the standard Oliver-Pharr [36] and the alternative Galanov-Dub [37] approaches are employed. The latter approach is based on the use of a refined analytical representation of the unloading branch of the indentation force-displacement curve (Figure 2). The refined approach takes approximately into account that during loading of the sample, the points of the sample surface within the contact region have irreversible displacements. The use of nanoindentation techniques enabled us to study properties of vitrinite and inertinite macerals separately. The questions related to anisotropy of the coal internal structure will be discussed in further publications. Results of hardness tests and depth-sensing indentation at micro and nanoscales are presented. The difference in behaviour of vitrinite and inertinite macerals of bituminous coals are described and compared with behaviour of anthracite samples.

It is argued that the current standard techniques of testing materials may be meaningless in application to coals. Indeed, it has been confirmed correctness of early observations [58] that during indentation, the integrity of the internal structure of a bituminous coal sample within a small area of high stress field near the tip of indenter may be destroyed. Therefore, both OP and GD approaches to coals may provide rather misleading results because the approaches were developed for testing materials whose internal structure is preserved during the loading-unloading cycle. On the other hand, these methods may be applied to anthracite that demonstrates practically ideal elastic behaviour during DSNI loading-unloading cycle.

To obtain quantitative estimations of the level of similarity between the shapes of load-displacement diagrams, it has been suggested to employ the parameter (R_W, %) that is the ratio between the hysteresis loop

of load-displacement diagrams (A_{hys}) to the full work of indenter tip at loading of the sample (A_{load}). It is shown that for low-rank bituminous coal samples, the average values of R_W are $34.2 \pm 1.5\%$ and $36.0 \pm 2.0\%$, at nanoindentation and microindentation respectively. For the inertinite maceral of these coals, the average values of R_W are $=41.0 \pm 1.3\%$ and $R_W = 45.3 \pm 1.0\%$ at nanoindentation and microindentation respectively. The values of this parameter for anthracite are 8:2±1.4% and 10.8±0:7% at nanoindentation and microindentation respectively. Thus, the load-displacement diagrams at nano and microscales are quite similar in all cases studied. However, for anthracite, there is no plastic imprints at nanoscale and it is very difficult to find any imprint at microscale, i.e. the values of P_{max} in our experiments were not large enough to create considerable imprint in the anthracite sample. The difference between loading and unloading branches is caused by internal damage of anthracite samples.

The values of hardness obtained in static experiments by the microhardness device are lower than the values obtained in DSNI tests. The hardness at nanoscale is relatively higher than the hardness found by microhardness DSI and static tests. Apparently, such effects are closely connected with varying of the crosslinks density between supramolecular clusters at different hierarchically organized structural levels of coals. This, in turn, indicates the decreasing of coals heterogeneity and defectiveness degree along with reduction of the studied volume during indentation tests at different scales.

Finally, it has been shown that the hardness values have strong correlation with the maximum load applied to the indenter and therefore, the microhardness tests that are parts of national standard tests for characterization of coals (see e.g. [15]), may be also meaningless for these materials. Thus, the mechanical behaviour of coals differs drastically from the behaviour of metals, plastics and other traditional materials, therefore the standard approaches of mechanical testing of coals should be re-examined.

References

1. R. C. Neavel, ACS Div. Fuel Chem. Prepr. 24 v 1, 73 (1979).
2. M. Klawitter, J. Esterle, and S. Collins, Int. J. Rock Mech. Min. Sci. 76, 237 (2015).
3. P. B. Hirsch, Proc. R. Soc. A Math. Phys. Eng. Sci. 226, 143 (1954).
4. Z. Zhao, W. Wang, C. Dai, and J. Yan, Trans. Nonferrous Met. Soc. China 24, 1538 (2014).
5. V. L. Shkuratnik, P. V. Nikolenko, and A. E. Koshelev, J. Min. Sci. 52, 873 (2016).
6. J. Pan, Z. Meng, Q. Hou, Y. Ju, and Y. Cao, J. Struct. Geol. 54, 129 (2013).
7. V. L. Shkuratnik, Y. L. Filimonov, and S. V. Kuchurin, J. Min. Sci. 41, 44 (2005).
8. V. L. Shkuratnik, Y. L. Filimonov, and S. V. Kuchurin, J. Min. Sci. 42, 203 (2006).

9. Y. Zhao, S. Liu, Y. Jiang, K. Wang, and Y. Huang, Rock Mech. Rock Eng. 49, 1709 (2016).

10. Y. Zhao, G.-F. Zhao, Y. Jiang, D. Elsworth, and Y. Huang, Int. J. Coal Geol. 132, 81 (2014).

11. R. D. West, G. Markevicius, V. M. Malhotra, and S. Hofer, Fuel 98, 213 (2012).

12. A. N. Korshunov, D. M. Dergunov, A. B. Logov, and B. L. Gerike, Sov. Min. Sci. 11, 571 (1975).

13. N. H. Macmillan and D. G. Rickerby, J. Mater. Sci. 14, 242 (1979).

14. B. Das, Int. J. Rock Mech. Min. Sci. 9, 783 (1972).

15. GOST 21206-75 Coals and Anthracite. Determination Method for Microhardness and Microbrittleness (1977).

16. V. L. Shkuratnik, Y. L. Filimonov, and S. V Kuchurin, J. Min. Sci. 40, 458 (2004).

17. A. Morcote, G. Mavko, and M. Prasad, Geophysics 75, E227 (2010).

18. X. Liu, F. Dai, and J. Liu, Comput. Model. New Technol. 18, 337 (2014).

19. V. L. Shkuratnik, Y. L. Filimonov, and S. V. Kuchurin, J. Appl. Mech. Tech. Phys. 47, 236 (2006).

20. A. O. Vatulyan, E. L. Kossovich, and D. K. Plotnikov, Mech. Solids 52, 429 (2017).

21. J. G. Speight, The Chemistry and Technology of Coal., 3rd ed. (CRC Press, New York, 2013).

22. J. Chen and S. J. Bull, J. Phys. D. Appl. Phys. 44, 1 (2011).

23. J. Chen, M. A. Birch, and S. J. Bull, J. Mater. Sci. Mater. Med. 21, 277 (2010).

24. E. Atar, C. Sarioglu, U. Demirler, E. Sabri Kayali, and H. Cimenoglu, Scr. Mater. 48, 1331 (2003).

25. L.-N. Zhu, B.-S. Xu, H.-D. Wang, and C.-B. Wang, Crit. Rev. Solid State Mater. Sci. 40, 77 (2015).

26. Khrushchov MM, Berkovich ES (1950) Devices PMT-2 and PMT-3 for microhardness testing. Izdatelstvo AN USSR, Moscow (in Russian)

27. M. M. Khruschchov and E. S. Berkovich, Izv. AN SSSR. Otd. Tekh. Nauk 1645 (1950). (in Russian)

28. ASTM E384: Standard Test Method for Microindentation Hardness of Materials (2016).

29. F. M. Borodich, S. J. Bull, and S. A. Epshtein, J. Min. Sci. 51, 1062 (2015).

30. S. A. Epshtein, F. M. Borodich, and S. J. Bull, Appl. Phys. A Mater. Sci. Process. 119, 325 (2015).

31. E. L. Kossovich, F. M. Borodich, S. J. Bull, and S. A. Epshtein, Thin Solid Films 619, 112 (2016).

32. A. Kounkov, GeoLines 22, 40 (2009).

33. E. L. Kossovich, N. N. Dobryakova, S. A. Epshtein, and D. S. Belov, J. Min. Sci. 52, 906 (2016).

34. E. Kossovich, S. A. Epshtein, N. Dobryakova, M. Minin, and D. Gavrilova, in Phys. Math. Model. Process. Geomedia 3d Int. Sci. Sch. Young Sci. Novemb. 01-03, 2017 (IPMech RAS, Moscow, 2018), pp. 4550.

35. E. L. Kossovich, S. A. Epshtein, V. L. Shkuratnik, and M. G. Minin, Gorn. Zhurnal 25 (2017).

36. W. C. Oliver and G. M. Pharr, J. Mater. Res. 7, 1564 (1992).

37. B. A. Galanov and S. N. Dub, J. Superhard Mater. 39, 373 (2017).

38. G. N. Kalei, Mashinovedenie 4, 105 (1968). (in Russian)

39. F. M. Borodich and L. M. Keer, Int. J. Solids Struct. 41, 2479 (2004).

40. F. M. Borodich, in Adv. Appl. Mech. (2014), pp. 225366.

41. M. M. Chaudhri, J. Appl. Phys. 124, 095107 (2018).

42. S. I. Bulychev, V. P. Alekhin, M. K. Shorshorov, A. P. Ternovskij, and G. D. Shnyrev, Zavod. Lab. 41, 1137 (1975).

43. W. C. Oliver and G. M. Pharr, J. Mater. Res. 19, 3 (2004).

44. B. A. Galanov, O. N. Grigorev, Y. V Milman, and I. P. Ragozin, Strength Mater. 15, 1624 (1983).

45. B. A. Galanov, O. N. Grigorev, Y. V Milman, I. P. Ragozin, and V. I. Trefilov, Dokl. Sov. Phys. 29, 146 (1984).

46. R. Y. Lo and D. B. Bogy, J. Mater. Res. 14, 2276 (1999).

47. J. C. Hay, A. Bolshakov, and G. M. Pharr, J. Mater. Res. 14, 2296 (1999).

48. S. Veprek, S. Mukherjee, H. D. Mnnling, and J. He, Mater. Sci. Eng. A 340, 292 (2003).

49. Y. P. Cao, M. Dao, and J. Lu, J. Mater. Res. 22, 1255 (2007).

50. M. G. J. Veprek-Heijman, R. G. Veprek, A. S. Argon, D. M. Parks, and S. Veprek, Surf. Coatings Technol. 203, 3385 (2009).

51. J. Hay, P. Agee, and E. Herbert, Exp. Tech. 34, 86 (2010).

52. F. M. Borodich, B. A. Galanov, L. M. Keer, and M. M. Suarez-Alvarez, Mech. Mater. 75, 34 (2014).

53. B. A. Galanov, Y. V Milman, S. I. Chugunova, and I. V Goncharova, J. Superhard Mater. 25 (1999).

54. L. A. Galin, Contact Problems (Springer Netherlands, Dordrecht, 2008).

55. A. N. Tikhonov and V. Y. Arsenin, Methods of Solving Ill-Posed Problems (Nauka, Moscow, 1979). (in Russian)

56. F. R. Gantmakher, The Theory of Matrices (Chelsea Pub. Co., New-York, 1960).

57. V. V. Voevodin, Linear Algebra (Nauka, Moscow, 1974). (in Russian)

58. I. I. Argatov, F. M. Borodich, S. A. Epshtein, and E. L. Kossovich, Mech. Mater. 114, 172 (2017).

59. J. D. Currey, Bones: Structure and Mechanics (Princeton University Press, Princeton, New York, 2002).

60. J. Y. Rho, L. Kuhn-Spearing, and P. Zioupos, Med. Eng. Phys. 20, 92 (1998).

61. D. Carnelli, P. Vena, M. Dao, C. Ortiz, and R. Contro, J. R. Soc. Interface 10, 20120953 (2013).

62. D. Carnelli, R. Lucchini, M. Ponzoni, R. Contro, and P. Vena, J. Biomech. 44, 1852 (2011).

63. M. Taffetani, M. Griebel, D. Gastaldi, S. M. M. Klisch, and P. Vena, J. Mech. Behav. Biomed. Mater. 32, 17 (2014).

64. J. Menčík, D. Munz, E. Quandt, E. R. Weppelmann, and M. V Swain, J. Mater. Res. 12, 2475 (1997).

65. J. Devore, Brooks/Cole 776 (2011).